Preprints of the 23rd IFAC World Congress
Busan, Republic of Korea, August 23-28, 2026

Identification of Non-linear Sloshing Dynamics Using Operational Manoeuvres ⋆

Emily Burgin * **Frederik Thiele** * **Charles Dehombreux** **
Benoit Garnier ** **Xavier Manuel Juanpere** ** **Harald Pfifer** *

* *Technische Universität Dresden, Dresden, Germany (e-mail: {emily.burgin, frederik.thiele, harald.pfifer}@tu-dresden.de).*
** *Airbus Defence and Space, Toulouse, France (e-mail: {charles.dehombreux, benoit.b.garnier, xavier.manuel-juanpere}@airbus.com)*

Abstract: Complex space systems exhibit non-linear dynamics that are unmodelled during the design phase. This can cause detrimental effects on performance after launch. On-board identification of these dynamics can be used to maximise operational performance and mitigate risk. This paper proposes an algorithm that identifies the non-linear dynamics of fuel sloshing using only on-board measurements acquired during normal operation. No additional excitation manoeuvres are used, thus conserving propellant and maintaining the mission timeline. The method uses an ℓ_1-regularised linear regression to determine the governing equations of the dynamics. The algorithm is demonstrated on a communication satellite with a dual-tank architecture and a chemical propulsion system. Real flight data, provided by Airbus Defence and Space, demonstrate the algorithm's applicability to industry-grade systems.

Keywords: Flight dynamics modelling and identification; guidance, navigation and control of aircraft and spacecraft; space exploration and transportation.

1. INTRODUCTION

This paper considers the identification of non-linear sloshing dynamics of a chemical telecommunications satellite (CTS) performing station keeping manoeuvres (SKM). These manoeuvres are characterised by a thrust command, resulting in acceleration-dominant sloshing behaviour. For this type of sloshing (with high Bond number), the behaviour is typically modelled with linear dynamics, for example using pendulum systems or mass spring dampers (see, e.g., Sharma et al. (2019); Dodge (2000); Abramson (1966)). However, flight data recorded during the SKM of a geostationary telecommunications satellite from Airbus' Eurostar product line were unable to be fitted by the conventional methods. Therefore, a novel identification approach is proposed in this paper that is able to capture the non-linear dynamic behaviour exhibited in the flight data.

The sloshing dynamics are coupled in feedback with the spacecraft dynamics. The latter are well known from ground tests or in-flight calibration. The former features time-varying and transient behaviours, whose physical states (associated to mechanical approximations) are not measured on-board. In addition, a full depiction of the internal model structure is difficult to derive a priori. This makes it a challenging identification problem. Moreover, specific excitation manoeuvres are prohibited during the mission due to fuel and operational constraints. Therefore, the identification procedure proposed in this work has to rely solely on operational manoeuvres. The proposed approach is to estimate the sloshing torque as the output from the sloshing dynamics and assume a non-linear canonical form of fixed order for the model structure. By choosing a set of suitable basis functions for the non-linearities, the identification turns into a linear regression problem.

Linear regression is commonly used in a wide range of system identification methods considering both linear and non-linear dynamics. A detailed overview is provided, for instance, in Ljung (1999). Similarly, these methods are often used to obtain surrogate models in linear fractional form, see Pfifer (2013); Hardier et al. (2013). In these applications, models of low complexity are usually favoured. In other words, the goal is to find a sparse solution to the linear regression. Thus, ℓ_1-regularised least square regression is preferable. More recently, the methods have been applied for the sparse identification of non-linear dynamics, see Brunton et al. (2016). This work builds upon these ideas and develops a method to identify dynamics characterised by measurable input-output behaviour. Then, the method is applied to the flight data from a real spacecraft mission.

Related works in the identification of spacecraft dynamics include application of neural network based approaches, which have been specifically applied to sloshing by Pizzoli et al. (2023). These methods are computationally very expensive and require large amounts of data for training. In the work of Elliott et al. (2025), unscented Kalman filters are used for the real-time identification of flexible

⋆ This work is supported by ESA under contract No. 4000146466/24/NL/CRS entitled On-Board System Identification on Real-time for Versatile AOCS.

©2026 the authors. Accepted by IFAC for publication under a Creative Commons Licence CC-BY-NC-ND

dynamics for robust control design. Kalman approaches are generally well regarded in the industry due to their flight heritage, however they require a good prior knowledge of the model structure and can be sensitive to initial tuning parameters.

The identification problem and proposed approach are described in detail in Section 3, followed by the application to flight data in Section 4.

2. PRELIMINARIES

2.1 Sparse Identification of Non-linear Dynamics

Assume a discrete, non-linear dynamical system of the form

$$x(k+1) = f(x(k), u(k)), \tag{1}$$

where the state vectors at the current and future time-step ($x(k) \in \mathbb{R}^{n_x}$ and $x(k+1) \in \mathbb{R}^{n_x}$ respectively) and the input vector $u(k) \in \mathbb{R}^{n_u}$ are measurable, but the function f is unknown. Under these assumptions finding a suitable candidate to approximate f amounts to solving a linear regression problem using measured data. The principal idea is to pick a set of known basis functions $\{f_i(x(k), u(k))\}_1^{n_b}$, where n_b is the number of basis functions. Common choices include trigonometric functions or monomials.

Consider input and state data that is sampled over a period of time, where m denotes the number of samples. Then for one state $x^{(j)}$, with $j \in \{1, n_x\}$ of the system (1) the following can be constructed from the data and basis functions

$$\underbrace{\begin{bmatrix} x^{(j)}(2) \\ x^{(j)}(3) \\ \vdots \\ x^{(j)}(m) \end{bmatrix}}_{X_{k+1}^{(j)}} = \underbrace{\begin{bmatrix} f_1(x(1),u(1)) & \cdots & f_{n_b}(x(1),u(1)) \\ f_1(x(2),u(2)) & \dots & f_{n_b}(x(2),u(2)) \\ \vdots & \ddots & \vdots \\ f_1(x(m-1),u(m-1)) & \cdots & f_{n_b}(x(m-1),u(m-1)) \end{bmatrix}}_{F(X_k,U_k)} \underbrace{\begin{bmatrix} b_1^{(j)} \\ b_2^{(j)} \\ \vdots \\ b_{n_b}^{(j)} \end{bmatrix}}_{b^{(j)}}, \tag{2}$$

where $F(X_k, U_k) \in \mathbb{R}^{(m-1)\times n_b}$ is the data matrix, which contains the chosen basis functions evaluated at the state sequence X_k and input sequence U_k. The state sequence X_k contains samples for all states. For one state it is $X_k^{(j)} = [x^{(j)}(1), \dots, x^{(j)}(m-1)]^T$, for $j = \{1, \dots, n_x\}$. The input sequence is constructed in the same fashion for all inputs $U_k^{(l)} = [u^{(l)}(1), \dots, u^{(l)}(m-1)]^T$, for $l = \{1, \dots, n_u\}$. The vector $X_{k+1}^{(j)}$ is the shifted state sequence that shall be fitted with linear regression to obtain the coefficient vector $b^{(j)}$ for the j-th state. In total, n_x regressions are solved, one for each non-linear state equation.

The common goal of identification is to find a balance between model complexity and accuracy. The complexity is hereby given by the number of non-zero entries in $b^{(j)}$. In other words, identification is to find a solution to a least squares problem with a sparse coefficient vector $b^{(j)}$, i.e, with a small cardinality $\text{card}(b^{(j)})$. In literature, this approach is referred to as SINDy (sparse identification of non-linear dynamics) and was originally proposed by Brunton et al. (2016). Until now, previously published works using SINDy exist in a continuous-time formulation.

2.2 ℓ_1-Regularised Least Squares

A good heuristics to approximate a least squares problem that also minimizes $\text{card}(b^{(j)})$ is ℓ_1-regularised least squares. It can be empirically seen that minimizing the ℓ_1-norm of a vector will also decrease its cardinality. Following the notation in (2), the ℓ_1-regularised least squares problem for one state can be written as

$$\min_{b^{(j)}} \left\| F b^{(j)} - X_{k+1}^{(j)} \right\|_2^2 + \lambda \left\| b^{(j)} \right\|_1. \tag{3}$$

In (3), $\left\|b^{(j)}\right\|_1 = \sum_{i=1}^{n_b} \left|b_i^{(j)}\right|$ is the ℓ_1-norm and $\lambda \geq 0$ the regularisation parameter, which presents a trade-off between $\text{card}(b^{(j)})$ and the residual $\left\| F b^{(j)} - X_{k+1}^{(j)} \right\|_2$. Various techniques exist in literature to solve the problem (3), e.g., coordinate descent (Friedman et al., 2007) or specialised interior-point methods Koh et al. (2007). The latter has been implemented in this paper.

3. IDENTIFICATION OF NON-LINEAR SLOSHING DYNAMICS

3.1 Identification Based on Measurable Outputs

Unlike the linear regression described in Brunton et al. (2016), the internal states, considered in the sloshing use-case, are not measurable. This is because they are related to the fluid position and velocity within the tank. The problem considered in this paper is more general than the one in Section 2.1. It assumes a non-linear dynamical system of the input-output form given below, with chosen relative degree r

$$y(k+r) = g(y(k+r-1), \dots, y(k), u(k+r-1), \dots, u(k)), \tag{4}$$

where the inputs $u(k) \in \mathbb{R}^{n_u}$ and outputs $y(k) \in \mathbb{R}^{n_y}$ of the system are measurable. This form (4) is known in literature as the NARX (Non-linear AutoRegressive model with eXogenous inputs) model (Billings and Leontaritis, 1982). The model can be adapted to be compatible with SINDy (Section 2.1) by introducing a new surrogate state vector z where $z(k) \in \mathbb{R}^{(n_y r)}$. For clarity, consider the system equation for one single output, denoted j: $y^{(j)}(k)$. Then the state vector is defined as

$$\underbrace{\begin{bmatrix} z_1^{(j)}(k) \\ z_2^{(j)}(k) \\ \vdots \\ z_r^{(j)}(k) \end{bmatrix}}_{z^{(j)}(k)} = \begin{bmatrix} y^{(j)}(k) \\ y^{(j)}(k+1) \\ \vdots \\ y^{(j)}(k+r-1) \end{bmatrix}. \tag{5}$$

The non-linear dynamical system (4) can then be written in the following form with the chosen output $y^{(j)}(k)$ as

$$\overbrace{\begin{bmatrix} z_1^{(j)}(k+1) \\ \vdots \\ z_{r-1}^{(j)}(k+1) \\ z_r^{(j)}(k+1) \end{bmatrix} = \begin{bmatrix} z_2^{(j)}(k) \\ \vdots \\ z_r^{(j)}(k) \\ \hat{f}^{(j)}(z(k), u(k)) \end{bmatrix}}^{z^{(j)}(k+1) = f^{(j)}(z(k), u(k))} \tag{6}$$

$$y^{(j)}(k) = z_1^{(j)}(k).$$

The identification of the input-output dynamical behaviour then reduces to finding the function $\hat{f}^{(j)}$. Given that $\hat{f}^{(j)}$ only depends on the measurable inputs u and the state vector z which is constructed from the measurable outputs y, $\hat{f}^{(j)}$ can be approximated analogous to Section 2.1 by choosing basis functions and using linear regression.

In more general terms, a regression is performed for each output $j = \{1, .., n_y\}$ of the original system (4) in order to find the coefficients $b^{(j)}$ in the following system equations

$$\begin{aligned} Z^{(j)}_{r,k+1} &= F(Z_k, U_k)b^{(j)} \\ Y^{(j)}_k &= Z^{(j)}_{r,k-r}. \end{aligned} \tag{7}$$

Here, F is constructed from input data, output data and basis functions. Consider one measured output vector $[y^{(j)}(1), \ldots, y^{(j)}(m)]$ and a chosen relative degree $r < m$. $Z_k \in \mathbb{R}^{(m-r)\times(n_y r)}$ contains time-series information on all states, stacked column-wise. For each output $j = \{1, ..., n_y\}$, $Z^{(j)}_k = [z^{(j)}(1), \ldots, z^{(j)}(m-r)]$, where $Z^{(j)}_k \in \mathbb{R}^{(m-r)\times n_y}$ and $z^{(j)}$ is defined in (5). Therefore, Z_k is constructed from only measurable outputs. The input $U_k \in \mathbb{R}^{(m-r)\times n_u}$ is defined in a similar way, containing time-series data from all inputs: $U^{(l)}_k = [u^{(l)}(1), \ldots, u^{(l)}(m-r)]$ for $l = \{1, ..., n_u\}$. The same notation applies to the output $Y^{(j)}_k \in \mathbb{R}^{(m-r)}$, i.e., $Y^{(j)}_k = [y^{(j)}(1), \ldots, y^{(j)}(m-r)]$. Similarly, using the definition of z_r (6), the output state vector to be fitted is $Z^{(j)}_{r,k+1} = [z^{(j)}_r(1+r), \ldots, z^{(j)}_r(m)]$; $Z^{(j)}_{r,k+1} \in \mathbb{R}^{(m-r)}$. Unlike the SINDy approach introduced in the previous section, for each output (j) only a single regression has to be calculated to obtain its respective $\hat{f}^{(j)}$ independent from the size of the state vector z.

Performing the regression to determine the governing equations of the system is referred to as *training*. In this work, it shall be demonstrated that after the *training* process the outputs to the system $y(k)$ can be propagated forward in time using only current input measurements $u(k)$. There is no need to continue to measure output data $y(k)$, and the state vector $z(k)$ is computed internally.

3.2 Problem Statement

Propellant sloshing is often among the major sources of concern during development of missions featuring chemical propulsion. Assessment of mission feasibility in such conditions is not straightforward, and traditionally relies on an iterative approach involving guidance profiles generation, computational fluid dynamics analyses, attitude & orbit control system (AOCS) analyses and design consolidation. In addition, when sloshing-induced disturbances are close to typical AOCS bandwidth frequencies, increasing the static controller gain to improve the rejection is not always possible; the solution is then to modify the propulsion architecture, which ultimately leads to a more costly design.

In this context, there is a growing interest in performing system identification to enable direct sloshing rejection, e.g. in a feed-forward scheme. This paper focuses on the identification part of this concept, targeting non-linear sloshing identification during station keeping manoeuvres of a CTS, depicted in Fig. 1. It also defines the satellite

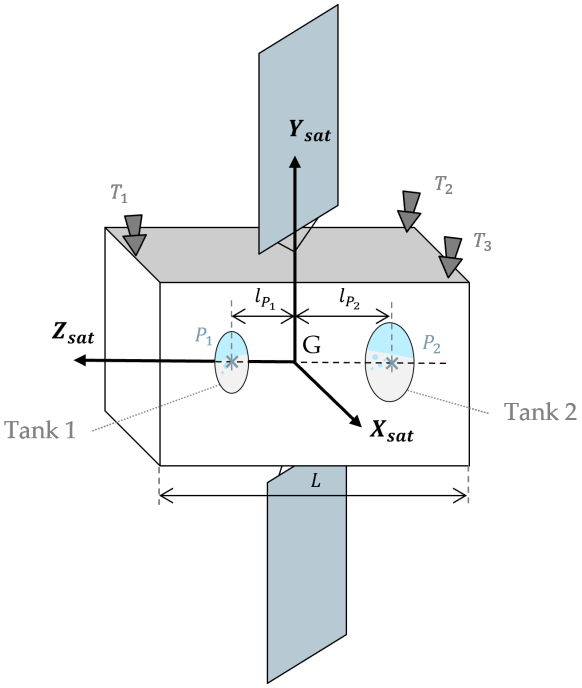


Fig. 1. Configuration of the bi-propellant CTS (not to scale)

Table 1. Applicable CTS sloshing parameters.

Parameter	**Value**
Tank 1 position along Z_{sat} (l_{P_1})	$0.1L$
Tank 2 position along Z_{sat} (l_{P_2})	$0.3L$
Tank 1 & 2 filling ratios	$\in$ [0.1, 0.4]
Tank 1 Bond number	$\in$ [40, 55]
Tank 2 Bond number	$\in$ [25, 35]

frame, whose origin is located at the centre of mass of the central rigid body. Tanks 1 and 2 are assumed membraneless. Both tank centres, P_1 and P_2, are located along Z_{sat}. Relevant configuration parameters, applicable to the flight data set that is used to generate results in this work, are provided in Table 1.

During operational station keeping manoeuvres, thrusters T_1 to T_3 generate a resulting force along the Y_{sat} axis, inducing sloshing effects. The resulting Bond number, expressed for each tank, describes the ratio between surface tension and acceleration-induced forces. In the considered case, this indicator clearly indicates an acceleration-dominated behaviour. Mission attitude is maintained thanks to combined actuation of reaction wheels and thrusters. Attitude and rate measurements are provided by a star tracker and gyrometer, respectively.

3.3 Sloshing Setup

This section presents the main contribution of this paper; the application of SINDy on a dynamical system with measurable input-output behaviour. The proposed method was used to identify the non-linear, acceleration-dominant sloshing dynamics of the bi-propellant CTS (Section 3.2). Following the explanation in Section 3.1, the dynamics to be identified are set-up as a non-linear second order system (i.e. $r = 2$). The chosen outputs (y) are disturbance torques that explicitly arise due to the sloshing

behaviour $\tau = [\tau_x^T\ \tau_y^T\ \tau_z^T]^T$; three disturbance torques expressed about each respective body frame axis. The considered inputs (u) are the control torque components, commanded by the reaction wheels, in the body frame $\tau_{ctl} = [\tau_{ctl,x}^T\ \tau_{ctl,y}^T\ \tau_{ctl,z}^T]^T$. These torques are calculated by an attitude controller in the form of a proportional-derivative controller. Additionally, a time vector t is included so that time-varying dynamics, expected due to the initial fluid acceleration and thrust transient, may be captured.

Therefore, using (6), the equation of the sloshing dynamics to be identified takes the form

$$\underbrace{\tau(k+2)}_{z_r(k+1)} = \hat{f}(\underbrace{\tau(k+1), \tau(k)}_{z(k)}, \underbrace{t(k), \tau_{ctl}(k)}_{u(k)}), \tag{8}$$

where $\hat{f}$ denotes the non-linear dynamic function of states and inputs that is computed from the chosen basis functions $\{f_i(z(k), u(k))\}_1^{n_b}$ and the solution b to the regression (3).

One challenge encountered with this real-world application is that disturbance torques are not directly measurable. Hence, the output data that is required for the identification process in this scenario must be reconstructed from measurable signals. Note that this computation is only needed for the *training* phase, once the governing equations are defined, measured outputs are no longer necessary. The output training data is computed using the principle that the total torque on the main body τ_{tot} is approximately equal to the sum of control torque τ_{ctl} and disturbance torque τ

$$\tau = \underbrace{J\dot{\omega} + \overbrace{\omega \times (J\omega)}^{\approx 0}}_{\tau_{tot}} - \tau_{ctl}. \tag{9}$$

Here, ω is the measured angular rate of the spacecraft that can be differentiated to compute the angular acceleration $\dot{\omega}$. The inertia matrix J is assumed constant. The non-linear term is neglected, as for this application, angular rates ω are small so the non-linearity is several orders of magnitude smaller than the linear terms. Note that there will be errors and noise introduced through the measured and processed quantities.

3.4 Algorithm

The algorithm to identify the governing equations is detailed in this subsection. The general workflow of this algorithm is broken into three steps: (1) measure and process the data (2) initialise the regression (3) perform the regression and compute the governing equations.

Step 1: Measure and process the data

To obtain a rich data set for the identification of the sloshing dynamics, five consecutive SKM are used in the regression. Recall that it is not possible to perform specific excitation manoeuvres on the spacecraft. To reconstruct the sloshing torques, see (9), the angular acceleration $\dot{\omega}$ is obtained by a filtered differentiation of the angular rate ω, measured by the gyrometer of the spacecraft. A second order low pass filter with a bandwidth of 0.47 rad/s (0.075 Hz) is used to reduce the impact of noise on the differentiation. This is well outside of the range of the observed sloshing bandwidth so the dynamics of sloshing are maintained in the data.

Step 2: Initialise the regression

The data matrix F is generated in accordance to Section 3.1. The measured input data of all five manoeuvres are stacked into a matrix $U_k \in \mathbb{R}^{n_m(m-r)\times n_u}$ where $n_m = 5$ is the number of manoeuvres, $n_m(m-r)$ the cumulated number of samples for the training data set and n_u the number of inputs. In this case $n_u = 4$, corresponding to the time vector t and the three control torques $\tau_{ctl,x}$, $\tau_{ctl,y}$ and $\tau_{ctl,z}$. Similarly, the measured output data from the manoeuvres is collected in the state data matrix $Z_k \in \mathbb{R}^{n_m(m-r)\times n_y r}$. The state data matrix Z_k contains the data of the three sloshing torques τ_x, τ_y and τ_z and their discrete derivatives up to degree 2, (since $r = 2$). The output state vector $Z_{r,k+1}$ is the time-step shifted data from $Z_{r,k}$, as described in Section 3. For each output j, the output state vector is denoted $Z_{r,k+1}^{(j)}$, where j corresponds to a set of r columns of Z_k (there are $n_y r$ columns in total) and $k+1$ denotes that the output is one step forward in time. Monomials up to second order are chosen as the basis functions $\{f_i(z(k), u(k))\}_1^{n_b}$. This is a common choice in literature and reflects the physical understanding of the system. A distinct disadvantage of monomials is that the data matrix F can easily become ill-conditioned for higher order monomials, see Lin (2006). Hence, they are restricted to second order in this paper.

For the following ℓ_1-regularised least squares problem, it is important that both the data matrix F and the state data $Z_{r,k+1}$ are normalised. Since the cardinality of the coefficient vector b is approximated by the ℓ_1-norm, normalisation ensures that negligible coefficients are accurately identified, see Efron et al. (2004); Pfifer and Hecker (2013). In the presented approach the data is normalised such that each column of $\tilde{F}$ and $\tilde{Z}_{r,k+1}$ have unit length and zero mean.

Step 3: Perform the regression and get the governing equations

The ℓ_1-regularised least squares regression is performed as in (3), with the normalised data matrix $\tilde{F}$ and state data vector $\tilde{Z}_{r,k+1}^{(j)}$. The regression problem is defined for each torque state $j = \{1, 2, 3\}$

$$\min_{\tilde{b}^{(j)}} \left\| \tilde{F}\tilde{b}^{(j)} - \tilde{Z}_{r,k+1}^{(j)} \right\|_2^2 + \lambda \left\| \tilde{b}^{(j)} \right\|_1. \tag{10}$$

with the regularisation parameter $\lambda = 0.05$. The regression is performed sequentially on the three sloshing torques, corresponding ot each j. After solving the ℓ_1-regularised least squares regression, normalised coefficients $\tilde{b}^{(j)}$ that are smaller than the chosen threshold (0.01) are set to zero and a final least squares fit only containing the non-zero elements in $\tilde{b}^{(j)}$ is performed. Finally, normalisation of the coefficients is reversed to obtain $b^{(j)}$ for each j. Together with the basis functions in F, this describes the governing equations of the sloshing dynamics.

4. RESULTS

The flight data exhibits a sloshing force transient in each tank, which results from the initial fluid acceleration. Given the geometry (Fig. 1), this transient is mostly seen on the X_{sat} pointing error whereas non-linear oscillations are mostly reflected on X_{sat} and Y_{sat} axes. Figure 2 shows a typical evolution of the thrust manoeuvre.

Figure 3 provides the training inputs (used to construct U_k) of the 5 manoeuvres. The training window (see Fig. 3) spans from the beginning of the data set to 500 seconds. The data is plotted to demonstrate that the measurements from the 5 training manoeuvres are unique to ensure that the learned governing equations will capture the general sloshing behaviour.

Verification of the governing equations was completed using a sixth manoeuvre, denoted *test manoeuvre*. The control torque $\tau_{ctl}(k)$ and current time $t(k)$ of the *test manoeuvre* are taken as the measured inputs $u(k)$, then the surrogate states are propagated forward in time from the governing equations $z_r(k{+}1) = \hat{f}(z(k), u(k))$, $y(k) = z_1(k)$ with a time-step of 0.125 s (equal to the time-step of the measured data and corresponding to the sampling frequency of the on-board algorithms).

In the comparison of the reconstructed sloshing torque and the estimated sloshing torque (Fig. 4), it can be seen that the algorithm is successfully capturing the dynamic behaviour of the non-linear sloshing. The normalised root mean square error (NRMSE) fitness for the first 600 seconds of data is 82.5% 95.7% and 96.6% for the three sloshing torques respectively. Before 150 seconds, the fit is slightly worse than after 150 seconds. This is the most complex part as it is where the transient torques occur. From a visual inspection it appears that the identified model output about Y_{sat}, in particular, is not reaching the correct magnitude for the faster oscillations. Although, it can be seen that the dynamics modes are clearly still present.

The normalised governing equations that were generated from the training set are

$$\begin{aligned}
\tau_x(k{+}2) &= 0.42\tau_x(k) + 0.42\tau_x(k{+}1) - 0.19\tau_{ctl,x}(k) \\
&\quad - 0.17\tau_x(k)t(k) - 0.013\tau_x(k)\tau_{ctl,y}(k) \\
&\quad - 0.17\tau_x(k{+}1)t(k) - 0.017\tau_x(k{+}1)\tau_{ctl,y}(k) \\
&\quad + 0.023\tau_{ctl,x}(k)\tau_{ctl,z}(k) - 0.049\tau_{ctl,y}(k)\tau_{ctl,y}(k) \\
\tau_y(k{+}2) &= 0.21\tau_y(k) - 0.031\tau_x(k{+}1) + 0.21\tau_y(k{+}1) \\
&\quad + 0.070\tau_{ctl,x}(k) - 0.098\tau_{ctl,y}(k) \\
&\quad - 0.036\tau_x(k{+}1)^2 + 0.027\tau_x(k{+}1)\tau_{ctl,x}(k) \\
\tau_z(k{+}2) &= -0.32\tau_{ctl,z}(k).
\end{aligned} \tag{11}$$

As explained in the setup of the regression, all terms with coefficients below the chosen threshold of 0.01 were removed to maintain sparsity. Note that the normalisation of the training data was reversed for implementation of the governing equations with measured data. This process is not shown here to maintain confidentiality of the identified system. Time-dependent terms only show up about X_{sat}. This is to be expected as the transient torques (i.e. time varying effects) have the strongest impact about the X_{sat}-axis. Interestingly, the sloshing torque about the Z_{sat}-axis

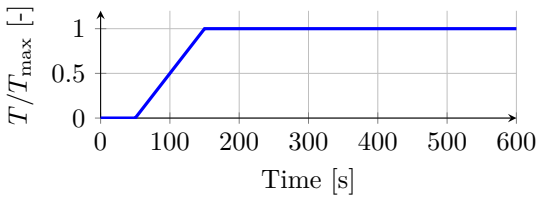


Fig. 2. Typical thrust profile, where T_{max} is the maximum thrust applied during the manoeuvre.

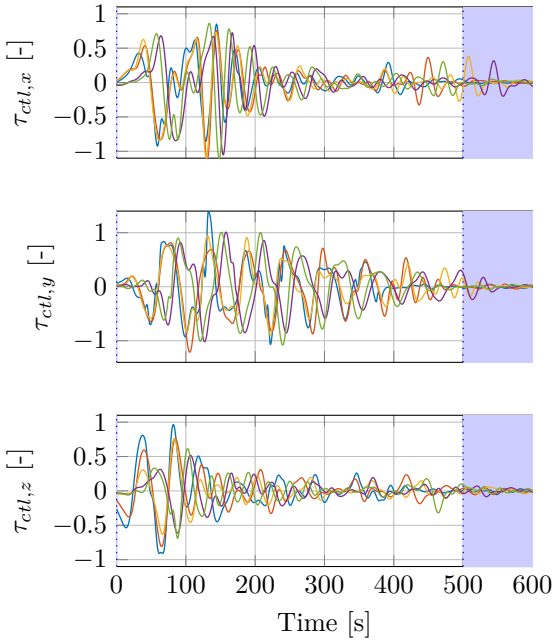


Fig. 3. Flight data training input signals. Data is scaled relative to the input data of the *test manoeuvre*.

is approximated as a scale factor of the control torque (with a time-step offset). This is logical, as the sloshing is barely seen in the closed loop system as the z-axis experiences the least amount of sloshing and it is already well compensated by the control torque.

It is important to note that the noise level in the output directly relates to the noise level in the control torque input signal τ_{ctl}. The equations are successfully identified without capturing the noise in the measurements.

5. CONCLUSION

A method for identifying non-linear sloshing behaviour from data measurable during operational manoeuvres was presented. The method does not rely on measurable internal states and is able to successfully capture the dynamic modes of the sloshing. The method was applied to flight data from a chemical telecommunications satellite performing station keeping manoeuvres. The identified non-linear equations have a low number of terms and reduced levels of noise compared to measured data.

ACKNOWLEDGEMENTS

The work described in this paper was carried out under the R&D OBSIRVA project and funded by the European

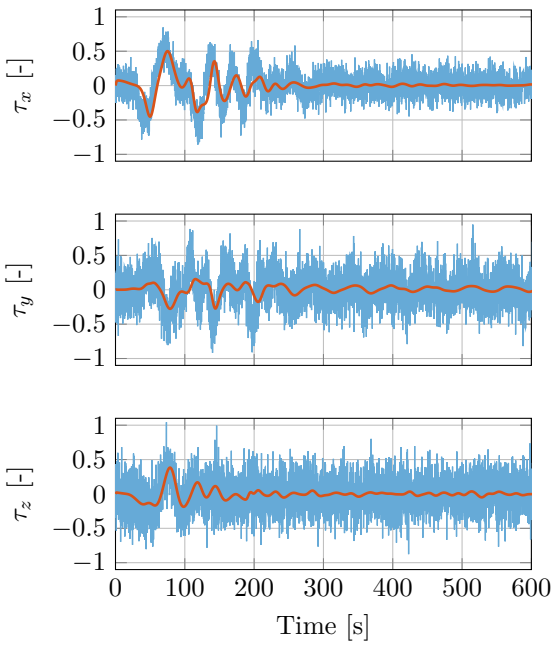


Fig. 4. Comparison of outputs computed from SINDy's governing equations (——) and measurements (——). Data is scaled to fit $\in [-1\ 1]$.

Space Agency (ESA): Technische Universität Dresden & Airbus would like to thank ESA for their trust in our technical teams to carry out such complex developments. Furthermore, the authors would like to thank the technical supervisor of the OBSIRVA project, Paul Acquatella, for his support, expertise and ongoing enthusiasm during the study. The views expressed herein can in no way be taken to reflect the official opinion of the European Space Agency.

DECLARATION OF GENERATIVE AI AND AI-ASSISTED TECHNOLOGIES IN THE WRITING PROCESS

During the preparation of this work the authors did not use any generative AI or AI-assisted technologies. The authors take full responsibility for the content of the publication.

REFERENCES

Abramson, H.N. (1966). The dynamics of liquids in moving containers. *NASA Report, SP*, 106, I960.

Billings, S. and Leontaritis, I. (1982). Parameter estimation techniques for nonlinear systems. *IFAC Proceedings Volumes*, 15(4), 505–510.

Brunton, S.L., Proctor, J.L., and Kutz, J.N. (2016). Discovering governing equations from data by sparse identification of nonlinear dynamical systems. *Proceedings of the national academy of sciences*, 113(15), 3932–3937.

Dodge, F.T. (2000). The new "dynamic behaviour of liquids in moving containers".

Efron, B., Hastie, T., Johnstone, I., and Tibshirani, R. (2004). Least angle regression. *The Annals of Statistics*, 32.

Elliott, A.J., Nakhaeezadeh Gutierrez, A., Felicetti, L., and Zanotti Fragonara, L. (2025). In-orbit system identification of a flexible satellite with variable mass using dual unscented kalman filters. *Acta Astronautica*, 226, 71–86. doi:https://doi.org/10.1016/j.actaastro.2024.11.014.

Friedman, J., Hastie, T., Höfling, H., and Tibshirani, R. (2007). Pathwise coordinate optimization.

Hardier, G., Roos, C., and Seren, C. (2013). Creating sparse rational approximations for linear fractional representations using surrogate modeling. *IFAC Proceedings Volumes*, 46(20), 399–404.

Koh, K., Kim, S.J., Boyd, S.P., et al. (2007). An interior-point method for large-scale l1-regularized logistic regression. *J. Mach. Learn. Res.*, 8(8), 1519–1555.

Lin, J.G. (2006). Modeling test responses by multivariable polynomials of higher degrees. *SIAM Journal on Scientific Computing*, 28(3), 832–867.

Ljung, L. (1999). *System Identification: Theory for the User*. Prentice Hall Information and System Sciences Series. Prentice Hall PTR, Upper Saddle River, NJ, 2nd ed edition.

Pfifer, H. (2013). *LPV/LFT Modeling and its Application in Aerospace*. Ph.D. thesis, Verlag Dr. Hut.

Pfifer, H. and Hecker, S. (2013). Lft model generation via l1-regularized least squares. In *Advances in Aerospace Guidance, Navigation and Control: Selected Papers of the Second CEAS Specialist Conference on Guidance, Navigation and Control*, 85–98. Springer.

Pizzoli, M., Saltari, F., Coppotelli, G., and Mastroddi, F. (2023). Neural network-based reduced-order modeling for nonlinear vertical sloshing with experimental validation. *Nonlinear Dynamics*, 111(10), 8913–8933. doi:10.1007/s11071-023-08323-y.

Sharma, V., Arun, C., and Krishna, I.P. (2019). The dynamics of liquids in moving containers. *Journal of Sound and Vibration*, 461, 114906.